Research Article

Shaobo Lü*, Ruisheng Wang, Jing Ma, Chao Jiang, Jiali Mu, Shuaifeng Zhao and Xiaojun Yin

Design and manufacture of super-multilayer optical filters based on PARMS technology

https://doi.org/10.1515/aot-2017-0075
Received November 17, 2017; accepted February 27, 2018; previously published online March 21, 2018

Abstract: Three multilayer interference optical filters, including a UV band-pass, a VIS dual-band-pass and a notch filter, were designed by using Ta_2O_5, Nb_2O_5, Al_2O_3 and SiO_2 as high- and low-index materials. During the design of the coating process, a hybrid optical monitoring and RATE-controlled layer thickness control scheme was adopted. The coating process was simulated by using the optical monitoring system (OMS) Simulator, and the simulation result indicated that the layer thickness can be controlled within an error of less than ±0.1%. The three filters were manufactured on a plasma-assisted reactive magnetic sputtering (PARMS) coating machine. The measurements indicate that for the UV band-pass filter, the peak transmittance is higher than 95% and the blocking density is better than OD6 in the 300–1100 nm region, whereas for the dual-band-pass filter, the center wavelength positioning accuracy of the two passbands are less than ±2 nm, the peak transmittance is higher than 95% and blocking density is better than OD6 in the 300–950 nm region. Finally, for the notch filter, the minimum transmittance rates are >90% and >94% in the visible and near infrared, respectively, and the blocking density is better than OD5.5 at 808 nm.

Keywords: dual-band-pass filter; notch filter; OMS; PARMS; UV band-pass filter.

1 Introduction

In recent years, with the development of life science, the requirement on the spectrum characteristics of optical filters has grown considerably. Especially on the effective spectrum range, the requirements for the transmission and blocking of precision optical filters that are used in biomedical analysis systems and instrument are very strict. For example, the demand for UV filters in fluorescence microscopes as its detecting area has expanded to the UV region and multiple-bandpass filters used in fluorescence detecting instruments in order to simplify the optical system and increase detecting channels. Typical requirements on these optical filters are high transmittance ($T_{avg} > 90$ or higher), sharp edge (<λ/100 from OD1 to OD6), deep blocking (OD > 6 in 300–1000 nm) and lower wave front distortion (<λ/4 for application of imaging fluorescence detection) [1, 2]. Moreover, in some fluorescence detecting systems with laser light source, notch filters are used to remove the laser energy mixed in the emitted light so as to increase the signal-to-noise ratio (SNR) and promote the accuracy of detection.

Therefore, the strict spectral characteristic of high transmittance, sharp edges and deep blocking ensure the high quality of the substrate, coating design, depositing technology and plant, etc. The purpose of this paper is to investigate the design of super-multilayer optical films and the manufacture of high-performance optical filters that can meet the optical requirements in fluorescence detecting instruments and realize the mass production of these filters.

2 Three optical filters

For all requirements mentioned above, three kinds of optical filters, including a UV band-pass filter for fluorescence microscopy [3], a VIS dual band-pass filter for fluorescence PCR [4] and an NIR 808 nm notch filter [5], were designed. All three filters were using one single substrate with both sides coated. An overview of the coating designs is shown in Table 1.

ESSENTIAL MACLEOD was used to simulate the sensitivity of the coatings to error and run 20 cases for each coating. The simulation result shows that the layer thickness errors are less than 0.3%, 0.1% and 0.2% for the three filters, respectively, so as to obtain

***Corresponding author: Shaobo Lü,** HB Optical, Shenyang Academy of Instrumentation Science Co., Ltd., Shenyang 110043, China, e-mail: lvshaobo@hb-optical.com
Ruisheng Wang, Jing Ma, Chao Jiang, Jiali Mu, Shuaifeng Zhao and Xiaojun Yin: Shenyang Academy of Instrumentation Science Co., Ltd., Shenyang, China

Table 1: Overview of the three filters' coating designs.

	UV BP	VIS dual BP	Notch filter
Materials	Ta_2O_5 SiO_2	Nb_2O_5 SiO_2	Al_2O_3 SiO_2
Coatings			
S1			
Layer Num	192	183	280
PTH/nm	17032	20577	34522
S2			
Layer Num	202	196	8
PTH/nm	19010	18535	360
Errors	<0.3%	<0.1%	<0.2%

good coating results. Complicated film stacks require the coating plant to deposit all the materials that are used in the designs, and the coating process should be very stable to ensure that the coated material has right optical constants. Moreover, the coating process monitoring system and method must be accurate enough to control the layer thickness within the right error tolerance that we needed.

3 PARMS coating technology and plant

A vacuum coating machine with plasma-assisted reactive magnetic sputtering (PARMS) technology, which is from Bühler Leybold Optics, was used to manufacture the three filters. PARMS coating technology uses a couple of magnetic controlled targets with MF power supply as the sputtering source and assisted with an RF power ECWR plasma source to deposit the coating materials [6, 7]. The PARMS coating plant has a series of advanced performances, such as stable coating process, fast deposition rate, high material packing density and consistency, to name a few, to ensure the coating process is completed accurately and efficiently.

The schematic diagram of the PARMS coating principle is shown in Figure 1. As can be seen, Ar and O_2 are used as the discharging gases in the process of PARMS deposition. Ar is related to the energy of ions for sputtering, which affects the packing density of the deposited material, and O_2 affects the composition of the deposited materials. A lambda sensor is used to monitor the oxygen proportion in the plasma during the coating process, and the discharge power is automatically regulated by PID controller to maintain the voltage at the lambda sensor constant. This ensures the stable oxidation state of the deposited layers [8].

The PARMS coating plant is equipped with the optical monitoring system OMS5100, which can realize the accurate control of a complex coating process. The single-wavelength monitoring method is integrated into the OMS5100 by measuring the transmittance of the monitoring chip in real time to monitor and control the thickness of the layers. The OMS5100 calculated the turning point of the transmission spectrum and corrected the stop point of the deposition process by Backward, Offset or forwarded algorithms in order to control the layer thickness accurately.

On the basis of the PARMS coating plant, we developed the coating processes for the following materials: Ta_2O_5, Nb_2O_5, Al_2O_3 and SiO_2. The process of the first three metal-oxide materials was controlled by the lambda sensor, whereas the SiO_2 was controlled by a constant sputtering power. In this way, the sputtering process is maintained at a stable deposition conditions to ensure that the deposited materials have the right optical constant. It is also important to define an appropriate deposition rate by adjusting the lambda sensor value to achieve higher control accuracy of the layer thicknesses.

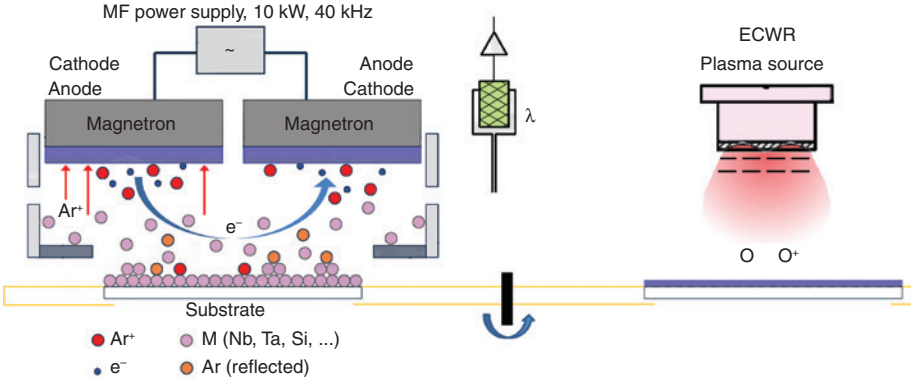

Figure 1: Schematic diagram of PARMS.

4 OMS coating process

All three filters were designed using a single substrate with coating on both sides, comprising a total of six coatings in all. The S2 coating of the VIS dual-band-pass filter is taken as an example to illustrate the optical monitoring system (OMS) coating process design. The processes of the remaining five coatings are similar to the S2 coating and are thus no longer introduced here in detail.

The design of the S2 coating of the VIS dual band-pass filter is based on the Fabry-Perot cavity. The basic design formula is given by

HLHL 2H LHLH L HLHL 4H LHLH L
(HLHL 6H LHLH L)^10
HLHL 4H LHLH L HLHL 2H LHLH L
1.2967(.5LH.5L)^28,

where H stands for Nb_2O_5, L stands for SiO_2 and the reference wavelength for the design is 687 nm. The design was optimized by using the ESSENTIAL MACLEOD to obtain a rectangular band-pass spectrum. During the definition of the optimization target, the requirements should not only contain the transmittance targets for the passband of the S2 coating, but also cover the wavelength region of another passband of the S1 coating. A similar optimization target definition is used in the S1 coating so as to ensure that both passbands have a good transmission.

4.1 Design of the OMS coating process

As shown in Table 1, the layer number of the S2 coating is 196, and the physical thickness is 18535 nm. To ensure that all these layers were deposited accurately, multi-chips monitoring strategy was adopted in design of the coating process. Given that all the layers are activated during the optimization, the quarterwave layers no longer feature the design and the turning point monitoring method cannot be used anymore. Thus, we divided the S2 coating into several parts, and each part with specified layers was coated using one monitoring chip. The whole coating is finished by using a plurality of monitoring chips.

For each sub-part of the coating on one monitoring chip, the selection of the appropriate monitoring wavelength and monitoring bandwidth is very important. The monitoring wavelength determines the monitoring curve of the coating process, especially its turning points and stop points, and also determines the selection of the thickness compensation algorithm for each layer. The monitoring bandwidth determines the detecting light intensity, so it should be wide enough to reduce the noise of detector and narrow enough to keep good monitoring accuracy at the same time. The two factors work together to determine the control precision of layer thickness in the coating process.

The monitoring wavelength should be close to the characteristic wavelength of the designed coating, such as the center wavelength or cut-off wavelength, which can help reduce or eliminate layer thickness error caused by material dispersion (in Figure 2, the first monitoring chip with layers 1–8). The monitoring wavelength should also make the stop point of the monitoring curve stay away (though not that far away from the turning point) so as to obtain a higher compensation accuracy. Additionally, in order to avoid the unstable intensity signal through the monitoring bandwidth, the monitoring wavelength should not be selected on the steep edge of the transmission spectrum of the current monitoring chip, because this can affect the layer thickness control accuracy.

Due to the different number of layers or physical thickness of each sub-part of the coating, the monitoring wavelengths for different monitoring chips may not be the same; even in a single chip, a single wavelength may not be able to complete the coating of all layers. Thus, we may have to set a different monitoring wavelength for each monitoring chip or change another monitoring wavelength at an appropriate layer position, which is called the multi-wavelength monitoring strategy. Figure 3 shows the optical monitoring curve of the first chip for the S2 coating. The monitoring wavelength is MWL = 620 nm.

The monitoring bandwidth should ensure that the detector in the OMS5100 can obtain high signal intensity, which is beneficial for the monitoring process while keeping the cut-off conditions stable and the noise level low. We should also make the monitoring bandwidth narrow enough to enable the OMS5100 to obtain higher

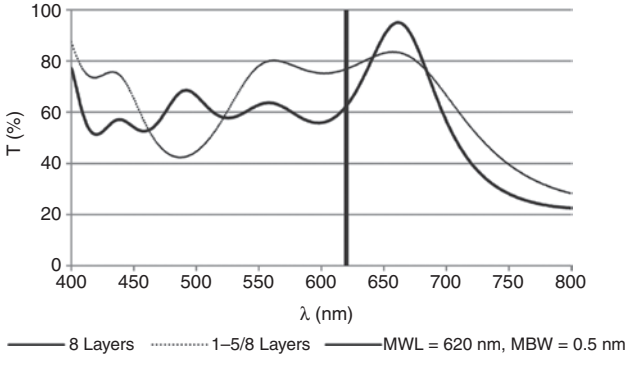

Figure 2: Sample of the monitoring wavelength for the OMS.

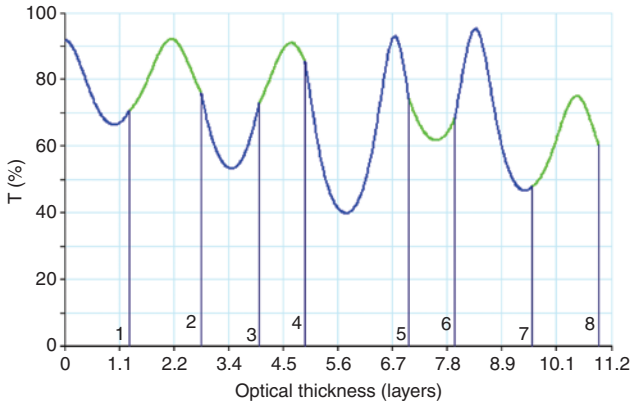

Figure 3: Monitoring transmittance curve of the OMS.

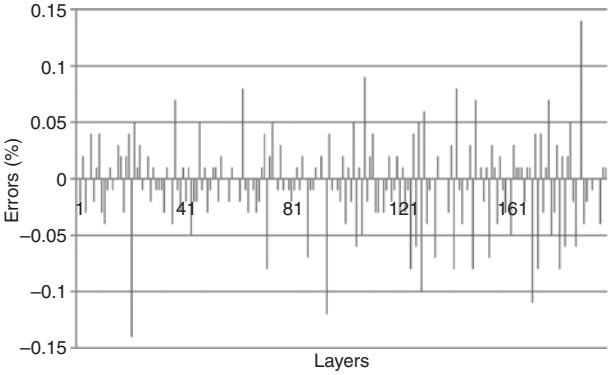

Figure 4: Layer thickness errors simulated by the OMS Simulator.

thickness control accuracy. As shown in Figure 2, the monitoring bandwidth is MBW = 0.5 nm. Furthermore, the monitoring transmittance curve is relatively gentle in the MBW region and the signal intensity is stable.

Due to the high control accuracy and thickness compensation effect between the layers, the direct optical monitoring should be chosen first as the coating process control method. However, if some of the layers cannot be coated under the current monitoring wavelength and bandwidth, the RATE control mode can be used to coat them. To complete the coating process, the RATE control mode takes the depositing rate of the last layer or the average rate of the last several layers, which is automatically calculated by the OMS5100, as the depositing rate of the current layer [9]. The premise of using the RATE control mode is that the discharging and coating process is very stable and smooth. We also note that the sputtering rate is affected by the lifetime of the targets, so only the adjacent last few layers' rates are effective and available.

To sum up the principles and considerations for designing an OMS coating process discussed above, we designed the PARMS coating process for the S2 coating of the VIS dual-band-pass filter as follows:

- Monitoring chips divided into: 8
- Min. MWL: 440 nm
- Max. MWL: 768 nm
- Monitoring bandwidth: 0.5nm
- Thickness compensation: BACKWARD
- OMS control: layers 1–195
- Rate control: layer 196

4.2 Simulation of the OMS coating process

To verify the feasibility of the designed OMS coating process, the OMS Simulator software, which is developed by Bühler Leybold Optics (Beijing, China), was used to simulate the process before running it on the coating machine. Different from the reverse engineering process [10], the parameters encoded into the Simulator are all from an actual coating process. This simulation considers almost all the errors that can possibly affect the coating process, such as random errors of the coating system, thickness linear errors, standard OMS noise deviation and some other factors, and then calculated and predicted the thickness error of each layer according to the designed OMS monitoring strategy.

After importing the coating process designed in Section 4.1 into the OMS Simulator, we set the deposition rate of Nb_2O_5 and SiO_2 as 0.5 nm/s, which is about the same as the actual depositing rate, after which we initiated the simulation. The simulation result is shown in Figure 4. As can be seen, most of the layers can be controlled within an error of less than 0.1%. For these layers with a slightly larger simulation error, we use the ESSENTIAL MACLEOD to calculate their sensitivity to errors. The result shows that even with an error of 0.2%, the coating can still maintain a good performance. This means that these layers are non-sensitive in the coating and their errors can be ignored.

We run this simulation thrice and the results are almost the same. The simulated transmittance spectrum also agrees fairly well with theory, as shown in Figure 5. This means that the designed coating process is feasible and reproducible. Hence, we can run it on the PARMS coating machine.

5 Coating performances

The three filters were all coated on a single K9 substrate with a diameter of 25.0 mm and a thickness of 2.5 mm. In the pre-conditioning of a coating process, the machine

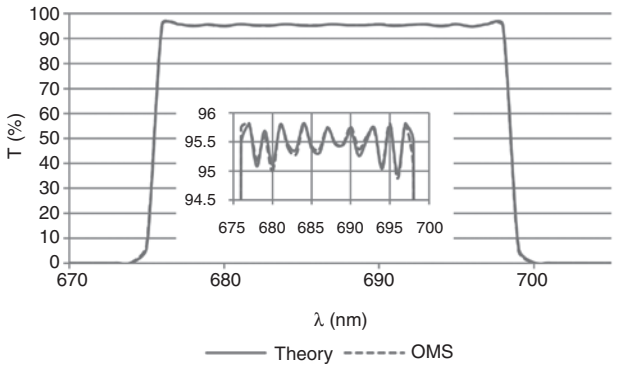

Figure 5: Simulated coating result of the OMS Simulator.

chamber was heated to 200°C and held for at least 20 min to remove the gas and moisture that adhered on the substrates. Next, the O^+ ion-beam generated from the ECWR plasma source was used to bombard the substrates for 120 s to perform a plasma cleaning of the substrates. This was followed by the actual coating process.

5.1 Coating performance of the UV band-pass filter

For the UV band-pass filter, Ta_2O_5 and SiO_2 were used as the coating materials. The theoretical spectrum specifications of this filter are CWL = 365 nm and FWHM = 48.7 nm; these are shown in Figure 6 as solid lines together with the blocking optical density.

In the design of the UV band-pass filter, the superposition structures of the long wavepass (LP) and short wavepass (SP) were adopted. The cut-on of the LP and the cut-off of the SP decide the slopes of the UV band-pass filter. The LP and SP film stacks interfere with each other to formulate the pass band. Due to the relative independence and mutual interference of the LP and SP film stacks, the FWHM of such kind of filter is difficult to control during production. However, because the LP + SP design is not too sensitive to thickness errors (about 0.3% as mentioned above), it is widely used in the design of the broadband-pass coatings.

The measuring results of the manufactured UV band-pass filter are as follows: CWL = 365.3 nm, FWHM = 47.1 nm and peak transmittance (T_{pk}) of about 97.7%, just as shown in Figure 6 in long-dash lines. The actual FWHM is about 1.6 nm narrower than the theoretical value, which is due to the independence of the LP and SP film stacks. The average blocking density is deeper than OD6 in the 300–1100 nm region, and the two thorn peaks of about OD 5.5–6.0 appear in the 900–1000 nm region. However, because the fluorescence excitation level of the detection reagent is very weak in this region, it can still satisfy the demand of fluorescence detection.

5.2 Coating performance of the VIS dual-band-pass filter

The theoretical spectrum specifications of the VIS dual-band-pass filter are as follows: CWL = 561 nm and FWHM = 35 nm for band 1 and CWL = 687 nm and FWHM = 23 nm for band 2. Nb_2O_5 and SiO_2 were adopted as coating materials. The theoretical and measured spectra of this filter are shown in Figure 7.

The Fabry-Perot cavity was adopted in the coating design of the dual-band-pass filter. Compared with the superposition structure of the LP and SP film stacks, the layer thickness tolerance of the Fabry-Perot cavity coating is very strict (0.1% as mentioned above). However, because the sharper cut-on and cut-off slopes can be easily achieved by using the Fabry-Perot cavity superposition, it is often used in the design of filters with very sharp edges.

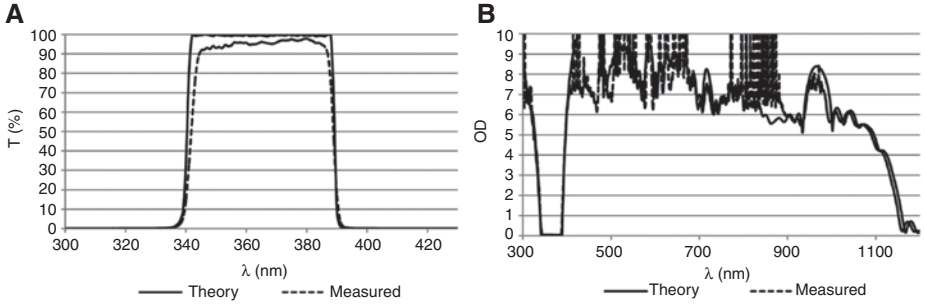

Figure 6: Transmittance and blocking curves of the UV band-pass optical filter. (A) Transmittance curve and (B) blocking curve.

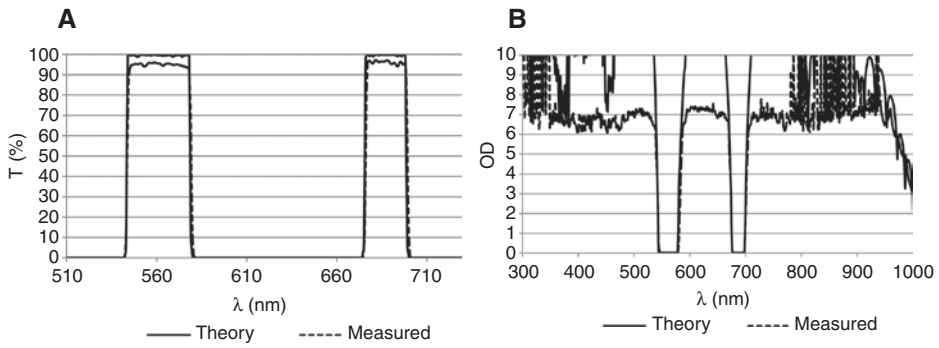

Figure 7: Transmittance and blocking curves of the VIS dual-band-pass optical filter. (A) Transmittance curve and (B) blocking curve.

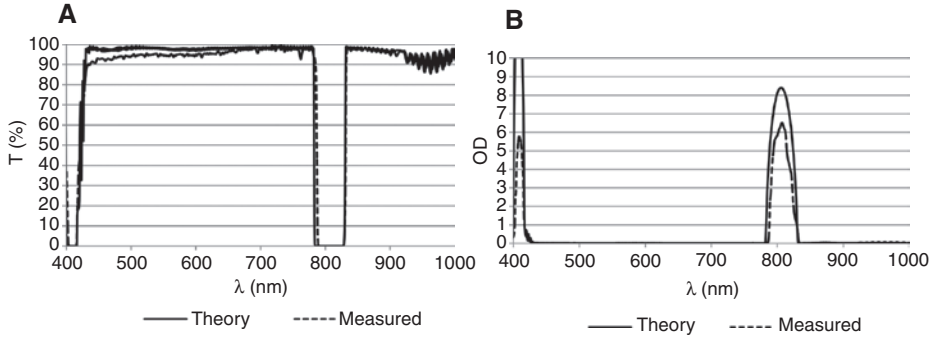

Figure 8: Transmittance and blocking curves of the 808-nm notch optical filter. (A) Transmittance curve and (B) blocking curve.

As shown in Figure 7, both bands of the dual-band-pass filter show good agreement between the theoretical curves and the measured results. For the first band CWL = 561.4 nm, FWHM = 35.4 nm and $T_{pk} > 97.2\%$, whereas for the second one, CWL = 687.5 nm, FWHM = 23.3 nm and $T_{pk} > 95.9\%$. The blocking density is deeper than OD6 in the 300–950 nm region. All the specifications that the filter achieved in the measurement can satisfy the requirements of the applications of fluorescence detection and analysis.

5.3 Coating performance of the NIR notch filter

The theoretical specifications of the 808 nm notch filter are as follows: average transmittance (T_{avg}) > 90% in the regions of 440–770 nm and 835–920 nm and blocking density > OD6 at 808 nm. The theoretical and measured spectra of this filter are shown in Figure 8.

For notch filters, the RUGATE designs with a small index contrast and apodization are well known in the literature. The required deposition of the gradient index layers or the so-called flip flop structures is very complicated and difficult to manufacture [11].

Thus, according to the required spectrum specifications, a formula structure of (A αB A)^m was adopted in the design of the 808 nm notch filter. The FWHM of the blocking region depends on the coefficient α, and the optical density of the blocking is determined by coefficient m. The materials with gradual refractive index is not needed in this design, and the thin layers can also be avoided during optimization. Moreover, the material combined with high refractive index contrast materials is not used in the design, because the refractive index of the combined material may not be able to maintain a constant value due to the changing sputtering rates, whether in one coating process or among different processes. Thus, in the design of the 808 nm notch filter, Al_2O_3 and SiO_2 were used as the coating materials, the thickness of the coating reached about 34.5 μm and the PARMS

coating machine was used to manufacture this filter. Figure 8 shows that in the specified wavelength region, the average transmittance is higher than 90% and blocking density is deeper than OD6 in region of 808 ± 3 nm, which can meet the required spectral specifications.

6 Conclusion

Three types of multilayer interference optical filters, including a UV band-pass filter, a VIS dual-band-pass filter and a NIR notch filter, were introduced in this paper. The PARMS coating technology and plant was used to manufacture the filters. The three filters all had the characteristics of superior multiple layers (more than 400 layers together on both side), large physical thickness (up to 34 μm) and ultra-low error tolerance (lower than <0.1%). The manufacturing results show that the OMS coating process based on PARMS can realize the production of the three filters. The spectrum characteristics of high transmittance ($T_{avg} > 90$ or higher) as well as deep and wide blocking (OD > 6 in 300–1100 nm) of the three filters can satisfy the spectrum requirement of fluorescence detection in modern biomedicine and life sciences.

References

[1] W. Ruisheng, L. Shaobo, Y. Xiaojun, Z. Shuaifeng and S. Yan, Selected Proceedings of the Chinese Society for Optical Engineering Conferences Held November, International Society for Optics and Photonics. 9796 (2016).
[2] Z. Weifeng, L. Buhong, X. Shusen, L. Yangzhong and Z. Chuanzhao, Laser Technol. 30, 123–125 (2006).
[3] Z. Huaxin, W. Tongtong, G. Jinsong, L. Guilin and L. Shuai, J. Synth. Cryst. 43, 1296–1301 (2014).
[4] W. Li, W. Zhanshan, W. Yonggang and C. Lingyan, Opt. Precis. Eng. 11, 643–646 (2003).
[5] M. Scherer, U. Schallenberg, H. Hagedorn, W. Lehnert, B. Romanov, et al. Proc. SPIE Int. Soc. Opt. Eng. 7101, 71010I-71010I-10 (2008).
[6] S. J. S. Jakobs, M. L. M. Lappschies, U. S. U. Schallenberg and O. S. O. Stenzel, Chin. Opt. Lett. 8, 73–77 (2009).
[7] V. Pervak, F. Krausz and A. Apolonski, Thin Solid Films. 515, 7984–7989 (2007).
[8] S. J. Pearce, M. D. B. Charlton, J. Hiltunen, J. Puustinen, J. Lappalainen, et al., Surf. Coat. Technol. 206, 4930–4939 (2012).
[9] B. Yikun, C. Kefu, Y. Ziqing, Z. Quan and Q. Longsheng, Laser & Infrared. 35, 968–970 (2005).
[10] T. V. Amotchkina, M. K. Trubetskov, V. Pervak, B. Romanov and A. V. Tikhonravov, Appl. Opt. 51, 5543–5551 (2012).
[11] Z. Baisen, M. Mianjun, X. Yuqing, C. Tao, W. Duoshu, et al. Vac. Cryog. 16, 219–222 (2010).